Environment International 167 (2022) 107404

Contents lists available at ScienceDirect

Environment International

journal homepage: www.elsevier.com/locate/envint

Full length article

# Distribution, behavior, and risk assessment of chlorinated paraffins in paddy plants throughout whole growth cycle

Xinyu Du [a,b,1], Bo Yuan [c,d,1], Jun Li [e,*], Ge Yin [f], Yanling Qiu [b], Jianfu Zhao [b], Xuchuan Duan [e], Yan Wu [g], Tian Lin [a], Yihui Zhou [b,*]

[a] College of Marine Ecology and Environment, Shanghai Ocean University, Shanghai 201306, China
[b] State Key Laboratory of Pollution Control and Resource Reuse, College of Environmental Science and Engineering, Tongji University, Shanghai 200092, China
[c] Department of Environmental Science, Stockholm University, SE-10691 Stockholm, Sweden
[d] Department of Chemistry, Norwegian University of Science and Technology, 7491 Trondheim, Norway
[e] School of the Earth Sciences and Resources, China University of Geosciences, Beijing 100083, China
[f] Shimadzu (China) Co., LTD, Shanghai 200233, China
[g] Key Laboratory of Geographic Information Science (Ministry of Education), School of Geographic Sciences, East China Normal University, Shanghai 200241, China

ARTICLE INFO

*Keywords:*
Paddy ecosystem
Chlorinated paraffins
Tissue distribution
Plant uptake modeling
Rice ingestion risks

ABSTRACT

Paddy plants provide staple food for 3 billion people worldwide. This study explores the environmental fate and behavior of a high-volume production emerging contaminants chlorinated paraffins (CPs) in the paddy ecosystem. Very-short-, short-, medium-, and long-chain CPs (vSCCPs, SCCPs, MCCPs, and LCCPs, respectively) were analyzed in specific tissue of paddy plants at four main growth stages and soils from the Yangtze River Delta, China throughout a full rice growing season. The total CP concentrations in the paddy roots, stalks, leaves, panicles, hulls, rice, and soils ranged from 181 to $1.74 \times 10^3$, 21.7–383, 19.6–585, 108–332, 245–470, 59.6–130, and 99.6–400 ng/g dry weight, respectively. The distribution profile indicated the translocation of SCCPs and MCCPs from soils to paddy tissue, highlighting their elevated bioaccumulative potential. The evolution of CP level/mass/pattern during the whole growth cycle suggested atmospheric CPs deposition on leaves and hulls, as well as stalk-rice transfer. CSOIL plant uptake model well predicted the level, distribution pattern, and bio-concentration factors (BCFs) of SCCPs and MCCPs in paddy shoot and recognized the soil-air-shoot pathway as the major contributor. Moreover, risk evaluation indicated that MCCPs intake and subsequent risks dominated the total exposure to CPs via rice ingestion. This is the first report on the occurrence, fate and risk assessment of all CPs classes in paddy ecosystems, and the results underline the potential health effects caused by the in-use MCCPs via rice ingestion.

## 1. Introduction

Chlorinated paraffins (CPs) are a group of high production volume chemicals with complex isomer composition. Technical CP products are cheaply manufactured via radical chlorination of alkane feedstocks (Tomy et al., 1998) and have been widely used as plasticizers, flame retardants, and lubricants in poly(vinyl chloride), rubber, metal working fluid, paint, and sealant products. CPs, based on their carbon chain length, are conventionally divided into very short-chain (vSCCPs, $C_{6\text{-}9}$), short-chain (SCCPs, $C_{10-13}$), medium-chain (MCCPs, $C_{14-17}$), and long-chain CPs (LCCPs, $C_{\geq 18}$). Among the four CP classes, SCCPs are of the most studied and have been regulated in 2017 under the Stockholm Convention (UNEP, 2017) since their PBT (persistent, bioaccumulative, and toxic) characteristics have been fully confirmed(van Mourik et al., 2016). MCCPs and LCCPs represent dominant ingredients (>50%) in current CP products(Du et al., 2018; Xia et al., 2021) and are expected to have mounting usage and environmental release upon the phase-out of SCCPs. With recent methodological improvement, the research hotspot has shifted to these in-use CP classes(Glüge et al., 2018) although the fundamental knowledge of their environmental fate and PBT features are yet to be well-investigated, especially for LCCPs(Yuan et al., 2019a). Recently, a novel CPs class, namely vSCCPs, occurred as byproducts and impurities (Xin et al., 2017; Yuan et al., 2017b) have been detected in various environmental matrices(Huang et al., 2017; Qiao et al., 2017;

* Corresponding authors.
*E-mail addresses:* junli@cugb.edu.cn (J. Li), jcapitalzyh@yahoo.com (Y. Zhou).
[1] These authors contributed equally to this research.

https://doi.org/10.1016/j.envint.2022.107404
Received 4 April 2022; Received in revised form 6 July 2022; Accepted 7 July 2022
Available online 15 July 2022

Qiao et al., 2018). Our previous studies reported their abundance in various biotas (Zhou et al., 2019) and found that vSCCPs shared comparable bioaccumulation characteristics with SCCPs (Du et al., 2020). These research findings warrant the need to study environmental processes of all CP classes as a whole.

Plants act as important sinks of persistent organic pollutants (POPs) and play a vital role in global POPs cycling (Gong et al., 2021). It has been well studied that plants can uptake several traditional POPs through air-foliar and soil-root pathways (Collins et al., 2006). However, limited research explored the occurrence and behavior of CPs in plants, most of which focused on SCCPs in pine needles and barks used as passive air samplers (Iozza et al., 2009; Wang et al., 2015a; Wang et al., 2016) and in plant seeds for food safety assessment (Cao et al., 2015; Yuan et al., 2017a). Very recently, Wang et al. (2021) investigated accumulation of SCCPs, MCCPs, and LCCPs in wetland plants and evaluated the CP removal efficiency by wetland systems. Chen et al. (2021a) studied the bioaccumulation and tissue distribution of SCCPs and MCCPs in mature maize plants near a CP production facility. Meanwhile, a series of single-standard spiking experiments investigated the transformation routes (e.g. chlorine rearrangement, dechlorination and carbon decomposition) of SCCPs in plants via hydroponic exposure (Li et al., 2020,2019,2017). More comprehensive research is urgently required to unveil the environmental behaviors of CPs in plants under different ecosystems and to elucidate the influence of human activities.

Rice (*Oryza sativa L.*) is one of the three major cereal crops contributing to 65% of the global staple food supply (Zhao et al., 2013). In China for example, paddy rice is particularly crucial for Chinese food safety since rice planting covered 30% of crop-cultivated area and comprised 40% of staple food production (Peng et al., 2008). Moreover, paddy fields undergo an unique dry-wet alternation during the whole cultivation cycle, which may significantly impact the fate of pollutants in paddy ecosystems (Li et al., 2015). Owing to the increasing concerns on food safety and ecological functions of paddy fields, there have been fruitful research on the environmental behavior of traditional POPs (e.g. PAHs, PCBs, and PBDEs) in paddy ecosystems and the associated risks (Chu et al. 1999; Li et al., 2015; Wang et al., 2015b), but the occurrence and fate of CPs in paddy fields remained scarcely studied.

In the present study, rice plants and soils were collected from a typical paddy fields in the Yangtze River Delta (YRD) during a full rice-growing season. vSCCPs, SCCPs, MCCPs, and LCCPs were determined in specific tissue of rice plants and paddy soils using an atmospheric pressure chemical ionization quadrupole time-of-flight mass spectrometer (APCI-QTOF-MS) method. We aim to (a) investigate the tissue distribution of CPs in paddy plants; (b) evaluate the behavior of CPs in paddies throughout the whole growth cycle; (c) estimate the potential CPs uptake pathways of paddy plants; and (d) assess the intakes and risks of CPs via rice ingestion. This is the first study on the occurrence, fate, and risk assessment of rice plants concerning all CPs classes.

## 2. Methods and materials

Detailed information on standards and reagents, sample information and sample treatment are given in supporting information (SI).

### 2.1. Sampling

The sampling sites were located at the junction of Shanghai and Jiaxing City in YRD, China. This area mainly comprises farming with limited industrial activities. Three paddy fields (over 100 m × 100 m) closely located within central agricultural area were hold by same farmer with the same cultivation process (wet in July and August and dry in September and October) and thus were selected as parallels. Paddy samples (*Oryza sativa L.*) were collected in the July, August, September, and October of 2012 spanning four main growth stages (seedling, tillering, heading, and mature stage) to represent the whole rice growth cycle. A total of 30 paddy plants were randomly sampled in each paddy field at each stage. Paddy soils were collected in the mature stage using the five-point sampling method and combined as three pool samples for each paddy field.

### 2.2. Analysis of CPs

The detailed procedures of sample pretreatment are provided elsewhere (Du et al., 2018). In brief, approximately 2 g (dry weight) of paddy tissue or soil sample, after spiked with 15 ng of $^{13}C_{10}$-1,5,5,6,6,10-hexachlorodecane ($^{13}$C-HCD), was Soxhlet extracted with 200 ml of dichloromethane/hexane (1:1, *v/v*) for 24 h. Copper was added for sulfur removal. The extracts were treated with concentrated sulfuric acid followed by acidic silica gel column. After then, neutral silica gel column was used to separate CPs from other polar compounds. The elutes were spiked with 5 ng of Dechlorane 603.

The instrumental methods and the quantification method were introduced in Du et al. (2020). In brief, CP homologue groups from $C_6Cl_4$ to $C_{31}Cl_{12}$ were screened using an APCI-QTOF-MS (QTOF Premier, Waters, Manchester, UK). The instrumental response factors of SCCPs, MCCPs, and LCCPs in the sample were calculated according to a linear combination of those of 20 CP products (Tables S1). The response factor of vSCCPs in the sample referred to a CP-52, the $C_{6\text{-}9}$ components of which was determined previously (Zhou et al., 2019). For schematic step-by-step quantification procedures see (Du et al., 2020).

### 2.3. Quality assurance/quality control

Procedural blanks were included with every five samples to monitor background contamination. The results were not blank corrected, given that the instrumental intensities of CPs in the samples with lowest concentrations (10th percentile) were on average 9 times more abundant than the blank (Fig. S1). Isotopically-labeled surrogate standard $^{13}$C-HCD was spiked in each sample to account for processing losses and matrix effects. Limits of detection and limits of quantification (LODs and LOQs, respectively) for vSCCPs, SCCPs, MCCPs, and LCCPs were calculated as average blank levels (n = 11) plus three or ten times the standard deviation of the blanks (SD), respectively (Table S2). The LOQ values of SCCPs and MCCPs mainly reflect their background levels during laboratory procedure. vSCCPs and LCCPs weren't detected in blanks and thus instrument detection limit was applied. Both *m/z* ratios and the isotopic abundances were used for resolving CP homologues (Yuan et al., 2016). The instrumental settings were optimized (Yuan et al., 2016) for balanced response factors among reference standards of different chlorine degrees. For example, the ratio between the response factors of SCCPs 63.0 %Cl and SCCPs 51.5 %Cl was merely 1.4 compared to 14 (Zou et al., 2018). The recoveries of surrogate standards were 98 ± 16% (87–121%) across all samples. The use of standards with single carbon chain length improved the performance of quantification method of linear combination of CP products ($R^2$ = 0.67–0.99, median $R^2$ = 0.92; Tables S1). The vSCCP homologue patterns for most samples (45 of 51, Table S3) were comparable to that of CP-52. When $R^2 < 0.50$, the vSCCP concentrations were reported as tentative values (Brandsma et al., 2017).

### 2.4. Plant uptake modeling

A bottom-up model named CSOIL was applied to simulate the accumulation of CPs by paddy shoot and identify the major uptake pathways in the mature stage using paddy soil data. Minor modifications in model structure and parameters were adopted to improve the model performance as described by Takaki et al. (2014) and the net direction of air–soil exchange of CPs was re-volatilization from soil to air according to the flux estimation. In the CSOIL model, uptake of CPs via root pathway depended on their flow amounts through root, which were closely associated with the stem transpiration rates and the water solubility of CPs (Trapp and Matthies, 1995). With regard to the soil-air

pathway, the air concentration of CPs was deduced by a volatilization model proposed by Jury et al. (1983) in which three volatilization fluxes (boundary layer flux, diffusion flux in soil, and the evaporation flux in soil water) were considered. Uptake via the particle pathway could be estimated based on a stable deposition rate and soil concentrations. In addition, the loss term of CPs within the shoot compartment included growth dilution and volatilization but not metabolism since reliable values for CP metabolism in plant was still very limited (biotransformation rate and major transformation pathway for CPs in plants remain unavailable). It is noteworthy that paddy shoot refers to all/anything aboveground part of mature paddies (including paddy leaf, stalk, rice, and hull) and thus the average data of these paddy tissues based on their mass were used as shoot data during model calculation. The model equations and detailed calculation procedures were described in the SI.

### 2.5. Risk assessment

Estimated daily intake of CP via rice ingestion ($EDI_{rice}$) was calculated as:

$$EDI_{rice} = \frac{C_{rice} M}{BW}$$

where C is the concentration of vSCCPs, SCCPs, MCCPs, and LCCPs in paddy rice (ng/g ww), M is the daily consumption of rice (g/day), and BW is the body weight. The daily consumption of rice was assumed to be 108 g/day and BW to be 57.3 kg for an local resident (Bureau, 2008).

Margin of exposure (MOE) was calculated as:

$$MOE = \frac{NOAEL}{EDI}$$

According to the risk assessment report of CPs by European Food Safety Agency (EFSA), no adverse effect level (NOAEL) of SCCPs, MCCPs, and LCCPs are 10, 10, and 1000 mg/kg bw per day, respectively (Schrenk et al., 2020). A total safety factor of 1000 was applied (Canada 1993). A health concern is suggested if MOE was below the safety factor.

Hazard quotient (HQ) (USEPA, 2000) was applied to assess exposure risks to four individual CP classes:

$$HQ = \frac{C_{rice}}{NOAEL}$$

The toxic risk proportion of four CP classes (HQ%) was defined as:

$$HQ\% = \frac{HQ}{HI} \times 100\%$$

where HI refers to Hazard Index, the sum of the HQs for all CP classes. Since no toxicity data is available for vSCCPs so far, NOAEL of SCCPs was applied for vSCCPs considering their similar physico-chemical properties.

### 2.6. Data analysis

The properties of targeted chemicals, including molecular weight, water solubility, vapor pressure, $K_{OW}$ and $K_{OA}$ values, were calculated by EPISuite (2012) and VEGA-QSAR Platform(Benfenati et al., 2013) (see Table S4). Statistical analysis was conducted by SPSS 22.0, and the significance level was set at $p < 0.05$.

## 3. Results and discussion

### 3.1. Occurrence and homologue patterns of CPs in paddy plants and soils

The concentrations of vSCCPs, SCCPs, MCCPs, and LCCPs in specific paddy tissue and soils are summarized in Fig. 1 and Table S5. SCCPs and MCCPs were detected in all the samples, while the detection frequencies of vSCCPs and LCCPs were 83.3% and 92.9%, respectively. The total CP levels (sum of vSCCP, SCCP, MCCP, and LCCP concentrations) in paddy roots, stalks, leaves, panicles, hulls, rice, and soils averaged at 982 ± 522, 129 ± 108, 273 ± 201, 195 ± 120, 333 ± 120, 89.6 ± 36.5 and 295 ± 170 ng/g dry weight (dw), respectively. In paddy root, stalk, rice grain, hull and soil samples, the concentrations decreased in the order of MCCPs > SCCPs > LCCPs > vSCCPs, while that of SCCPs > MCCPs > LCCPs > vSCCPs was found in paddy leaf and panicle samples. SCCPs and MCCPs were two dominant CPs groups contributing to 30.6–70.5% and 26.9–65.1% of the total CP levels, respectively. It is noteworthy that the summed proportions of SCCPs and MCCPs in paddy plants (up to 96.0%) were moderately higher than that in soils (86.2%), suggesting their plant accumulative potentials from soil.

The levels of SCCPs and MCCPs in rice plants herein (mature paddy shoot SCCPs 77.9 ± 38.2 ng/g dw; MCCPs 83.0 ± 34.7 ng/g dw) were comparable to those in wetland plants (SCCPs 127 ± 116 ng/g dw; MCCPs 289 ± 148 ng/g dw) from Beijing, China (Wang et al., 2021) but lower than those in pine needles from Chinese urban cities (Beijing: SCCPs 1090 ng/g dw; Shanghai: MCCPs 677 ng/g dw) (Wang et al., 2015a; Wang et al., 2016) and plant leaves collected from a CP production and e-waste area in China (maize: SCCPs 381 ng/g dw, MCCPs 551 ng/g dw; conifer: SCCPs 784 ± 496 ng/g dw, MCCPs 1749 ± 1126 ng/g dw) (Chen et al., 2018; Chen et al., 2021a). Only one research reported LCCP levels in whole wetland plants (from an artificial wetland receiving treated domestic wastewater in central Beijing) to be 188 ± 116 ng/g dw (Wang et al., 2021), which was one magnitude higher than our observations (mature paddy shoot 4.03 ± 2.26 ng/g dw).

The CP homologue patterns (from $C_6Cl_4$ to $C_{35}Cl_{16}$) as well as carbon and chlorine patterns in individual paddy tissue and soils are provided in Fig. 2 and S2-S4. In most samples, the dominant vSCCP alkane chain

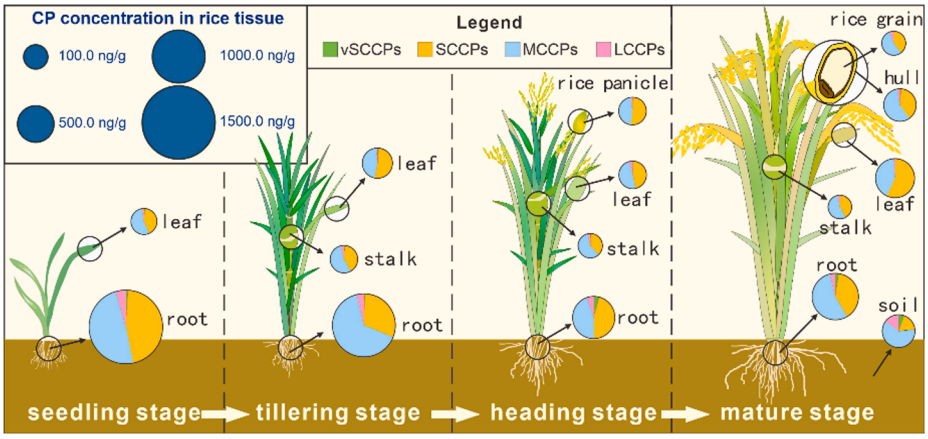


**Fig. 1.** Occurrence of vSCCPs, SCCPs, MCCPs, and LCCPs in paddy plants during the whole rice growth cycle.

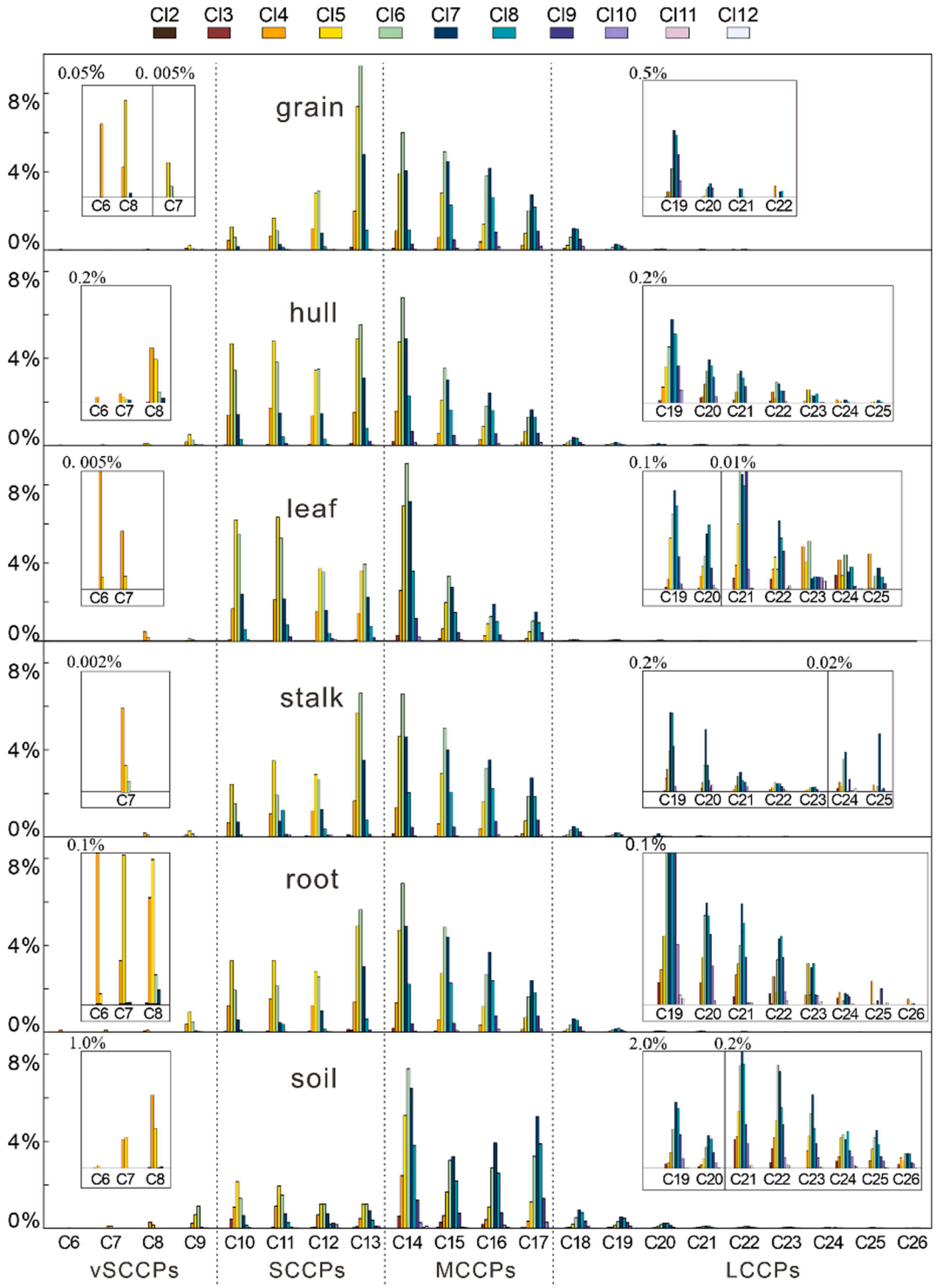


**Fig. 2.** Homologue patterns of CPs ($C_{6\text{-}26}Cl_{2\text{-}12}$) in paddy tissues and soil during mature stage. All the vertical axes represent response percent relative abundance; all the horizontal axes represent number of carbon atoms.

length groups were $C_9$ (61.9%) followed by $C_8$ (31.4%). The exception was for paddy leaves in early stages (seedling and tillering stage), in which vSCCPs were dominated by $C_8$ (58.3%). Different vSCCPs patterns suggested difference (Li et al., 2019) in fate and metabolism among vSCCPs carbon chain groups in plants and thus further research is needed. The dominance of $C_9$ was in line with our previous study on YRD wildlife but the proportion of $C_9$ in YRD wildlife were higher (up to 85.0%) (Zhou et al., 2019). In paddy root, stalk, panicle, hull and rice samples, the most abundant SCCP alkane chain length groups were $C_{13}$ (40.2%) while shorter carbon chain groups was dominated in paddy leaves ($C_{11}$, 28.3%) and soils ($C_{10}$, 28.8%). The dominance of $C_{10\text{-}11}$ were also reported in plant leaves and pine needles from other regions (Chen et al., 2021a; Wang et al., 2015a). For MCCPs and LCCPs, the predominant alkane chain length groups in all samples were $C_{14}$ (44.3%) and $C_{18}$ (59.7%), respectively, consistent with the profiles previously found in various biotic and abiotic matrices (Du et al., 2019; Glüge et al., 2018), suggesting their prevalence in CP products and elevated bio-accumulative potentials over other MCCPs and LCCPs. With regards to

chlorine pattern, $Cl_6$ (30.7%) was dominant in most samples followed by $Cl_5$ (26.9%). Incidentally, the alike chlorine pattern was frequently reported in plant, air samples, and other environment compartments around the world (Li et al., 2012; Wang et al., 2016; Yuan et al., 2021b).

### 3.2. Tissue distribution of CPs in mature paddy plants

In the mature stage of paddy fields, the total CP levels followed the order of root > leaf ≈ hull > soil > rice ≈ stalk (Fig. 1 and Table S5). Plant roots accumulated the highest total CP concentrations (610 ng/g dw) which was 1.7–7.0 folds of other paddy tissue and 2.1 folds of paddy soils. This could be caused by the direct translocation of organic pollutant by root from soil, and their tight relationship was exhibited in the result of principle component analysis (Fig. S5). Elevated POPs burdens in roots were frequently observed in laboratory and field studies (Li et al., 2017; Zhang et al., 2015). In contrast, plant stalks had the lowest CP concentration (86.9 ng/g dw) among all plant tissue. Low stalk levels and high root levels in mature paddy plants suggest the difficulty in acropetal translocation of CPs from root to stalk even though the root translocation was the major contributor of CPs in stalk. Similar root-stalk partitioning patterns of polyhalogenated compounds were detected in suburban paddy fields from the Pearl River Delta, China (Li et al., 2015; Zhang et al., 2015). CP concentrations in paddy hulls were 3.7 times higher than those in rice grains, agreeing with the profile reported for SCCPs in paddies from Taizhou, China (Yuan et al., 2017a). Paddy hulls had a larger surface area and thus can sorb more CPs from air, acting as an ideal passive sampler capturing organic pollutants (Fu et al., 2012), which was similar to the case of leaf (Fig. S5). Chen et al. (2021a) reported significantly higher SCCPs and MCCPs levels in mature maize tissue that directly contact with air (e.g. leaf and stalk) compared to maize roots, which was attributed to the atmospheric deposition of CPs from the CP production facility nearby. The different tissue distribution patterns between maize and paddy may be due to variations in CP sources and/or inter-species variations.

Regarding homologue patterns (Fig. 2), both paddy root and stalk contained high proportions of MCCP homologues, in line with the PCA results (Fig. S5). In contrast, paddy leaves and hulls were enriched in homologues with shorter carbon chains ($C_{10\text{-}11}$) (Fig. S5) probably originated from atmospheric CPs (Li et al., 2012). The different homologues between paddy stalk and leaves may be due to their different functions. Mature paddy leaves mainly function as photosynthesis and respiration so that they could sorb more atmospheric CPs compared with paddy stalks. Rice grains had unique patterns, where $C_{13\text{-}17}$ CPs contributed to 80% of the total CPs. It is noteworthy that paddy soils exhibited scattered carbon chain patterns with relatively higher composition of vSCCPs (3.67%) and LCCPs (9.73%) compared to paddy tissue (vSCCPs 1.31%; LCCPs 2.65%). Short alkane chain CP groups, particularly vSCCPs, were quite volatile and may evaporate and metabolize in plants(Li et al., 2019; Yuan et al., 2021b), while long alkane chain CPs (LCCPs) with large molecular size can be strongly bound with soil particles leading to very low bioavailability(Du et al., 2021). The appreciable enrichment of SCCPs and MCCPs from soils to paddy plants highlights their bioaccumulative potential as well as ecological risks via food chain transfer and human health effects through rice ingestion.

### 3.3. Evolution of CPs in paddy plants during the whole growth cycle

The variations of CPs concentrations and homologue patterns in paddy plants during the whole growth cycle (including four major growth stages) are shown in Figs. 2, S2–S4, and S6. In general, decreasing trends in CP levels were observed in plant root and stalk tissue throughout the growing season while the CP concentrations in paddy leaves gained with rice growth (Fig. S6). CP levels in all the tissue dropped from tillering stage to heading stage. Paddy plants continuously grow and the growth rate is relatively high during tillering and heading stage and their body mass surges. The dropping CP levels was probably due to the growth dilution while increase of leaf concentration indicated sorption of external CPs during growth. Regarding homologue patterns, tissue distributions of paddy plants in the early stages were similar to that of mature stages with relatively higher composition of shorter carbon chain patterns. No significant fluctuation was observed in paddy root and stalk tissue during the rice growth period. In contrast, the proportion of SCCPs in paddy leaves significantly increased from 40.8% (seedling stage) to 69.2% (heading stage). The CP homologue of rice seedling leaves (shoots) was similar with rice seedling roots (Fig. S2), suggesting common CPs origin(s) between root and leaves in seedling stage (probably soil–plant pathways). With the growth and development of paddies, leaf tissue tended to accumulate more short carbon chain CPs probably due to sorption of atmospheric CPs.

To further investigate the apportionment of CPs in paddies during rice growth cycle, the mass of four CP groups (ng/plant) in rice plant tissue during four growing stages were calculated and shown in Fig. 3. Total CPs mass in rice plants steadily increased from 270 ng/plant to 1300 ng/plant throughout the whole growing season. This means that after transplant a rice plant could assimilate nearly 1 μg CPs from abiotic matrices of paddy fields till harvest. Among all CP groups SCCPs and MCCPs together contributed to up to 96.0% of total CPs mass in paddy

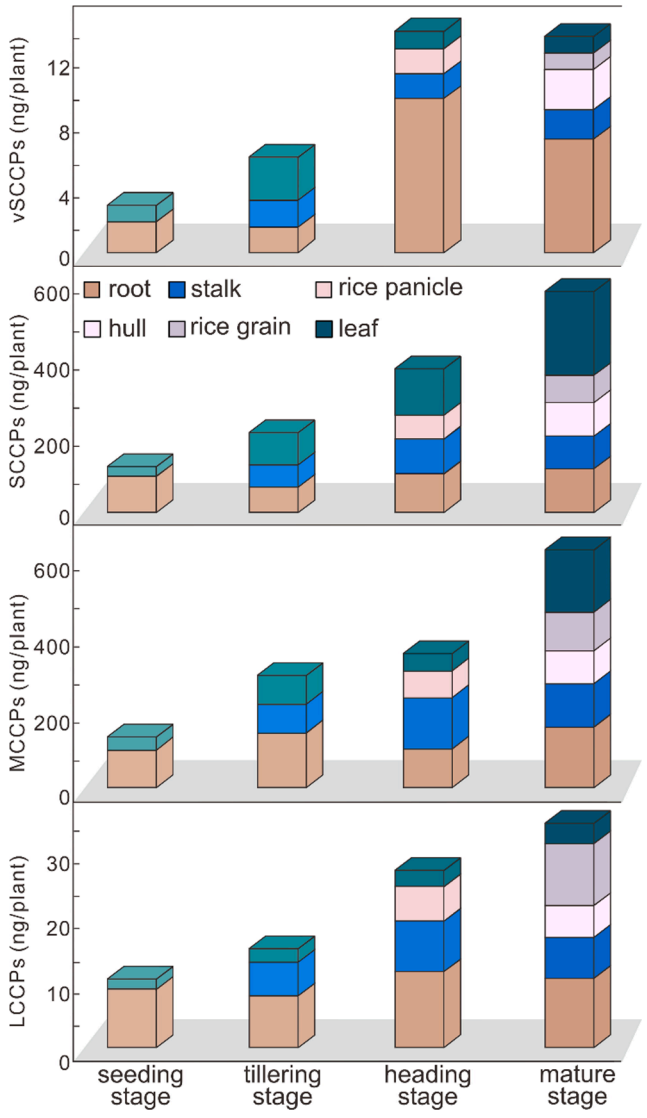


**Fig. 3.** Tissue-specific CP mass (ng/plant) of rice plants during whole rice growth period.

plants. The mass increment of SCCPs and MCCPs after four-stage growth was 460 ng/plant and 540 ng/plant, respectively. No significant mass alteration was observed in paddy root and stalks while SCCPs and MCCPs mass in paddy leaves steadily rose during the whole growth period. The comparable mass increment and tissue-specific evolution patterns highlighted similar environmental fate between SCCPs and MCCPs in paddies during rice growing periods. Although LCCPs mass also had an increasing trend, the absolute mass increment was very low (25.1 ng/plant) indicating their modest bioavailability. vSCCPs exhibited different growing patterns with a dramatic raise from tillering stage (5.76 ng/plant) to heading stage (13.6 ng/plant). Most of the mass increment came from paddy roots. One possible explanation is that the considerable mass increase of vSCCPs might be caused by the enhanced carbon decomposition of SCCPs in soil-root systems under aerobic condition. From tillering to heading stage the paddy cultivation mode changed from drawn mode into dry mode making the paddy fields shifted from anaerobic to aerobic condition. It is well known that aerobic systems have relatively high microbial amount, activity, and functional diversity causing high microbial metabolic capacity in soil-root systems. To date, limited information is available on the plant uptake and biotransformation of vSCCPs which needs further study.

Paddy leaves exhibited increasing CP level/mass and enrichment of short carbon chain CPs with rice growth. The mass increment of SCCPs, MCCPs, and LCCPs in paddy leaves after a cultivation cycle was 190, 150, and 1.44 ng/plant, respectively. Moreover, hydroponic experiments found that most SCCPs absorbed by plants from spiking cultured solution were stored in roots suggesting limited acropetal translocation (Li et al., 2017). Putting together, it can be concluded that paddy leaves continuously absorb atmospheric CPs with the growth of paddies. Paddy hulls shared similar SCCPs-dominated patterns and mass increment contribution of CP groups with paddy leaves, suggesting similar atmospheric origin of CPs. With the paddy growth, leaf and hull organs gradually have bigger surface area leading to greater sorption of organic pollutants from ambient air. Like paddy leaves, paddy stalks were expected to adsorb atmospheric CPs during rice growth leading to CP mass increment. In the mature stage, an unexpected CP mass decrease was observed in paddy stalks (from 236 to 210 ng/g plant). It is well-known that the nutrients (e.g. proteins) are firstly formed and stored in the above part of paddy plants before rice seed settling and then transported to rice grains (Xu et al., 2008; Zhao-Wei et al., 2009). Therefore, the slight drop of CP mass in paddy stalks may be due to the partitioning of CPs towards rice grains. Likewise, significant mass drop of MeHg in paddy stalks during rice ripen was also reported for paddy fields from Southwestern China (Meng et al., 2011). Close CP homologue patterns between paddy stalk and rice in mature stage further supported the stalk-rice transport. However, it should be noted that rice grains accumulated 184 ng CPs (mostly $C_{13\text{-}17}$) per plant, far more than the mass decrease observed in paddy stalks. Other processes (e.g., leaf-rice transport, atmospheric adsorption, transpiration of short carbon chain CPs) may also occurred in paddies during rice ripen, and thus further investigations are warranted.

### 3.4. Plant uptake modeling of CPs

In general, there are three main pathways controlling plant uptake of POPs from contaminated soils to shoot, including soil-root-shoot (root pathway), soil-air-shoot (soil-air pathway), and soil-particle-shoot (particle pathway). However, the dominant pathway for CP uptake in paddy is not clear, even though the soil-to-crop transfer of CPs has become a concern in food safety research (Chen et al., 2021). A bottom-up model named CSOIL was therefore used to evaluate the accumulation of CPs by paddy shoots and identify the major uptake pathways (see detailed calculation procedures in SI).

The exchange flux of soil-air system was firstly estimated using currently measured and previously published data (Liu et al., 2020). Results showed that the soil-air exchange flux of SCCPs and MCCPs (15.1 μg/$m^2$/day, direction from soil to air) was one order of magnitude higher than the wet/dry deposition flux of SCCPs and MCCPs (<1.49 μg/$m^2$/day) in the sampling area (see detailed calculation in SI). This suggested the dominance of volatilization of CPs in the air–soil interface and verify the hypothesis of soil-air-plant pathway for the model.

Using the CSOIL model that took into account the contributions from three pathways, the shoot concentration of CPs (caused by root uptake) and soil-air/particle depositions over a soil spiked with 295 ng/g dw CPs (measured paddy soil average level) was determined. Our model simulation showed that the soil-air pathway contributed more than 95.0% to the paddy uptake of vSCCPs, SCCPs and MCCPs, suggesting the importance of soil-air pathway for CP accumulation in paddy tissue, whereas uptake via the root pathway was kinetically limited likely due to the low concentration of CPs in freely dissolved phase, since the uptake of hydrophobic chemicals by roots and translocation to shoots was mainly dependent on their freely dissolved concentrations. The dominant contributor was subsequently shifted to particle deposition for $C_{20\text{-}26}$ LCCPs homologues with log $K_{ow}$ values higher than 11, consistent with previous findings (Takaki et al., 2014; Yuan et al., 2021b). The difficulty in desorbing these chemicals from soil compartments and partitioning towards air/water phases may result in very low bioaccumulative potential (Table S4). However, compared to our field study, the CSOIL model likely underestimated shoot uptake of LCCPs (Fig. 4a). The inconsistency was probably attributed to the uncertainty in the particle-deposition constant. In fact, the constant value can be up to 0.26 (Collins and Finnegan, 2010) and was tenfold more than the currently used value (0.01, CSOIL default), which profoundly affect the simulations of plant uptake for less volatized LCCP homologues.

The BCF value of each CP homologue was also estimated by the CSOIL model and compared with the experimental data in this study (Table 1). According to the model prediction, the BCF values steadily declined from vSCCPs to LCCPs with increasing log $K_{OA}$ values (Table S4). Among them, the BCF values of SCCPs and MCCPs (1.77 and 0.594) were close to their experimental observations (1.54 and 0.456), highlighting the bioconcentrating tendency for SCCPs while the dilution for MCCPs. The consistency between modelled and experimental results was also found for the relative abundance of SCCP and MCCP homologues (Fig. 4a). Hence, the CSOIL model well explained the outdoor experimental observations for shoot uptake of SCCPs and MCCPs in the paddy-soil system. However, we also noticed significant differences in the BCF values of vSCCPs and LCCPs between our simulations and observations. The CSOIL model overpredicted the bioaccumulation potential of vSCCPs ($BCF_{modelled} = 1.96$ *versus* $BCF_{experimental} = 0.127$). This probably reflected homologue-specific dilution of vSCCPs or high metabolic capability in soil-paddy system, albeit that in-soil decomposition of vSCCPs was rarely investigated. In contrast, the BCF value of LCCPs was simulated to be 0.0408, significantly lower than the value (0.167) from measured data. The possible underestimate in LCCPs uptake via particle pathway as mentioned above was probably a predominant factor driving such discrepancy. The other potential confounding factors include the uncertainties in chemical properties of LCCP homologues, such as $K_{ow}$ and $K_{aw}$ values. The hydrophobicity of LCCPs in real paddy ecosystem may be lower than the estimates used in our model simulation, since previous study reported the similar bioaccumulative potentials between some SCCP and LCCP homologues (Du et al., 2020). The knowledge gap in CP metabolism and properties might interfere with the accuracy of the model performance. Nevertheless, it seemingly predicted the overall trends in plant uptake (Fig. 4b, $r2 = 0.77$, $p < 0.01$) and the BCF value of CPs in our paddy-soil system (Table 1).

### 3.5. Risk assessment of CPs via rice ingestion

In the present study, the average and maximum concentration of CPs in paddy rice were utilized for risk characterization and the results are presented in Table 2. The average EDIs of vSCCPs, SCCPs, MCCPs, and LCCPs via rice ingestion were 1.32, 77.8, 110, and 10.4 ng $kg^{-1}$-BW $d^{-1}$,

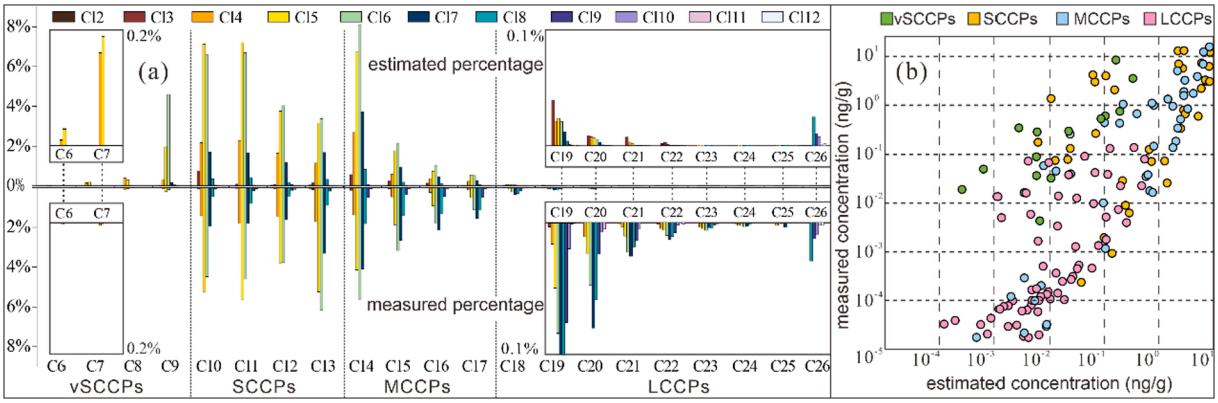


**Fig. 4.** Comparison of predicted pattern (a) and concentration (b) of CP homologues with measured ones in paddy shoot (all/anything aboveground part of paddies) during mature stage using CSOIL models.

**Table 1**
Modeling and observed data of BCF value and shoot concentration[a] (ng/g dw) for paddy plants.

| | Model simulations | | Observation data | |
|---|---|---|---|---|
| | BCF value | shoot concentration | BCF value | shoot concentration |
| vSCCPs | 1.96 | 15.1 | 0.127 | 0.971 |
| SCCPs | 1.77 | 107 | 1.54 | 92.7 |
| MCCPs | 0.594 | 122 | 0.456 | 94.7 |
| LCCPs | 0.0408 | 0.954 | 0.167 | 3.71 |

[a] Paddy shoot concentration was calculated as the average concentration of all/anything aboveground part of mature paddies including paddy leaf, stalk, rice, and hull based on their mass.

**Table 2**
Estimated exposure risks of CPs for residents via rice ingestion.

| | vSCCPs | SCCPs | MCCPs | LCCPs |
|---|---|---|---|---|
| $EDI^a_{avg}$ | 1.32 | 77.8 | 110 | 10.4 |
| $EDI^a_{max}$ | 1.47 | 112 | 160 | 15.9 |
| $MOE^b_{avg}$ | $7.58 \times 10^6$ | $1.29 \times 10^5$ | $9.12 \times 10^4$ | $9.64 \times 10^7$ |
| $MOE^b_{max}$ | $6.78 \times 10^6$ | $8.95 \times 10^4$ | $6.27 \times 10^4$ | $6.30 \times 10^7$ |
| HQ% | 0.699% | 41.2% | 58.0% | 0.0549% |

[a]Unit: ng $kg^{-1}$ BW $d^{-1}$.
[b]Unitless.

respectively. The EDI of SCCPs was comparable to the data reported for rice from Taizhou, China (26.4–297 ng $kg^{-1}$-BW $d^{-1}$) (Yuan et al., 2017a). The mean EDIs of SCCPs and MCCPs via maize kernel ingestion near a CP production facility was 8.94 and 5.01 ng $kg^{-1}$-BW $d^{-1}$, respectively (Chen et al., 2021a), one order of magnitude lower than our results. Interestingly, in that study other maize tissue had higher CP burdens (e.g., leaf: SCCPs 119–62,000 ng/g dw; MCCPs 77.6–52,900 ng/g dw) than our paddy tissue. This indicated that rice may accumulate more CPs in its fruit compared with other grain crops, causing higher risks of CP exposure.

Margin of exposure (MOE) approach was applied to assess rice ingestion risks caused by four CP classes. As shown in Table 2, the $MOE_{max}$ of vSCCPs, SCCPs, MCCPs, and LCCPs were at least one order magnitude greater than 1000, indicating no appreciable risks via rice ingestion when concerning four CP classes separately. To further investigate the toxic risk contribution of four CP classes, hazard quotient (HQ) was calculated and the risk proportions of four CP classes (HQ%) were illustrated (Table 2). MCCPs and SCCPs contributed to 58.0% and 41.2% of the total risks caused by rice ingestion, respectively while vSCCPs and LCCPs accounted for <1.00% of the total risks. Our results indicated MCCPs may pose more risks via rice ingestion compared with SCCPs while the health effect caused by LCCPs and vSCCPs could be trivial.

### 3.6. Environmental implications on global regulation

The present study unraveled the occurrence and fate of all CP classes in paddy fields during whole rice growth cycle. Our results indicated that SCCPs and MCCPs had considerable plant accumulation potential, shared similar environmental fate in paddy ecosystems, and contributed to most rice ingestion risks among all CP classes. Since SCCPs would be regulated globally by the end of 2022, the in-use MCCPs (now under evaluation by the POPs Review Committee) should be considered as the CP class of emerging concern which needs continuous routine monitoring and further regulatory action. LCCPs, another in-use class, exhibited poor plant bioavailability, trivial rice ingestion risks, and low biomagnification potential (Du et al., 2020) (especially for very long chain part $C_{>20}$) based on our observations. However, previous researches reported the dominance of LCCPs in wildlife (e.g. peregrine falcon (Yuan et al., 2019b) and killer whale (Yuan et al., 2021a) from Scandinavian region) and their long range transport to the arctic (Yuan et al., 2021a), suggesting that LCCPs might cause similar risks as SCCPs/MCCPs, and required equivalent regulation (Zhou et al., 2020). As main ingredient of commercial CP products, the global ban on LCCPs (likely after the ban on MCCPs) may lead to fully alternation of global CP industries (with production capacity of 1,900,000 t/year (Glüge et al., 2016)), causing considerable economic losses. Further comprehensive studies and careful evaluations on LCCPs are urgently warranted to rationalize present conflicted findings before making official political decision. At this point the decision makers could treat the two in-use CP classes differently when considering policies in risk evaluation.

## CRediT authorship contribution statement

**Xinyu Du:** Conceptualization, Writing – original draft, Formal analysis. **Bo Yuan:** Methodology, Writing – original draft, Validation. **Jun Li:** Conceptualization, Software, Supervision. **Ge Yin:** Writing – review & editing. **Yanling Qiu:** Resources. **Jianfu Zhao:** Supervision. **Xuchuan Duan:** Software. **Yan Wu:** Writing – review & editing. **Tian Lin:** Funding acquisition. **Yihui Zhou:** Supervision, Funding acquisition, Project administration.

## Declaration of Competing Interest

The authors declare that they have no known competing financial interests or personal relationships that could have appeared to influence the work reported in this paper.

## Acknowledgement

Prof. Michael McLachlan (Department of Environmental Science, Stockholm University) are gratefully acknowledged for his helping with data interpretation and uptake modelling. We thank Dr. Ziye Zheng (Cytiva Sweden AB) for statistical analysis and calculation of chemical properties. This study was financially supported by the National Natural Science Foundation of China (42107400, 42103085, 42107391), Shanghai Sailing Program (21YF1416900), the Foundation of Key Laboratory of Yangtze River Water Environment, Ministry of Education (Tongji University), China (YRWEF202107), and the Swedish Research Council (639-2013-6913).

## Appendix A. Supplementary material

Supplementary data to this article can be found online at https://doi.org/10.1016/j.envint.2022.107404.

## References

Estimation Programs Interface Suite™ for Microsoft® Windows, v 4.11 US EPA, Washington, DC, USA; 2012.

Benfenati, E., Manganaro, A., Gini, G., 2013. VEGA-QSAR: AI inside a platform for predictive toxicology. In: Proceedings of Workshop PAI, Turin Italy.

Brandsma, S.H., van Mourik, L., O'Brien, J.W., Eaglesham, G., Leonards, P.E.G., de Boer, J., Gallen, C., Mueller, J., Gaus, C., Bogdal, C., 2017. Medium-chain chlorinated paraffins (CPs) dominate in Australian sewage sludge. Environ. Sci. Technol. 51 (6), 3364–3372.

Bureau, S.M.S., 2008. Statistical yearbook of Shanghai.

Canada, E., 1993. Canadian Environmental Protection Act: Priority Substances List Assessment Report Chlorinated Paraffins.

Cao, Y., Harada, K.H., Liu, W., Yan, J., Zhao, C., Niisoe, T., Adachi, A., Fujii, Y., Nouda, C., Takasuga, T., Koizumi, A., 2015. Short-chain chlorinated paraffins in cooking oil and related products from China. Chemosphere 138, 104–111.

Schrenk, D., Bignami, M., Bodin, L., Chipman, J.K., del Mazo, J., Grasl-Kraupp, B., Hogstrand, C., Hoogenboom, L.(., Leblanc, J.-C., Nebbia, C.S., Ntzani, E., Petersen, A., Sand, S., Schwerdtle, T., Vleminckx, C., Wallace, H., Brüschweiler, B., Leonards, P., Rose, M., Binaglia, M., Horváth, Z., Ramos Bordajandi, L., Nielsen, E., 2020. Risk assessment of chlorinated paraffins in feed and food. EFSA J. 18 (3) https://doi.org/10.2903/j.efsa:2020.5991.

Chen, H., Lam, J.C.W., Zhu, M., Wang, F., Zhou, W., Du, B., Zeng, L., Zeng, E.Y., 2018. Combined effects of dust and dietary exposure of occupational workers and local residents to short- and medium-chain chlorinated Paraffins in a mega e-waste recycling industrial park in South China. Environ. Sci. Technol. 52, 11510–11519.

Chen, W., Hou, X., Liu, Y., Hu, X., Liu, J., Schnoor, J.L., Jiang, G., 2021. Medium- and short-chain chlorinated paraffins in mature maize plants and corresponding agricultural soils. Environ. Sci. Technol. 55 (8), 4669–4678.

Chu, S., Cai, M., Xu, X., 1999. Soil-plant transfer of polychlorinated biphenyls in paddy fields. Sci. Total Environ. 234 (1-3), 119–126.

Collins, C., Fryer, M., Grosso, A., 2006. Plant uptake of non ionic organic chemicals. Environ. Sci. Technol. 40 (1), 45–52.

Collins, C.D., Finnegan, E., 2010. Modeling the plant uptake of organic chemicals, including the soil− air− plant pathway. Environ. Sci. Technol. 44 (3), 998–1003.

Du, X., Yuan, B.o., Zhou, Y., de Wit, C.A., Zheng, Z., Yin, G.e., 2020. Chlorinated Paraffins in two snake species from the Yangtze river delta: tissue distribution and biomagnification. Environ. Sci. Technol. 54 (5), 2753–2762.

Du, X., Yuan, B.o., Zhou, Y., Zheng, Z., Wu, Y., Qiu, Y., Zhao, J., Yin, G.e., 2019. Tissue-specific accumulation, sexual difference, and maternal transfer of chlorinated Paraffins in black-spotted frogs. Environ. Sci. Technol. 53 (9), 4739–4746.

Du, X., Zhou, Y., Li, J., Wu, Y., Zheng, Z., Yin, G.e., Qiu, Y., Zhao, J., Yuan, G., 2021. Evaluating oral and inhalation bioaccessibility of indoor dust-borne short- and median-chain chlorinated paraffins using in vitro Tenax-assisted physiologically based method. J. Hazard. Mater. 402, 123449. https://doi.org/10.1016/j.jhazmat.2020.123449.

Du, X., Yuan, B.o., Zhou, Y., Benskin, J.P., Qiu, Y., Yin, G.e., Zhao, J., 2018. Short-, medium-, and long-chain chlorinated Paraffins in wildlife from paddy fields in the Yangtze river delta. Environ. Sci. Technol. 52 (3), 1072–1080.

Fu, J., Wang, T., Wang, P.u., Qu, G., Wang, Y., Zhang, Q., Zhang, A., Jiang, G., 2012. Temporal trends (2005–2009) of PCDD/Fs, PCBs, PBDEs in rice hulls from an e-waste dismantling area after stricter environmental regulations. Chemosphere 88 (3), 330–335.

Glüge, J., Schinkel, L., Hungerbühler, K., Cariou, R., Bogdal, C., 2018. Environmental risks of Medium-Chain Chlorinated Paraffins (MCCPs): a review. Environ. Sci. Technol. 52 (12), 6743–6760.

Glüge, J., Wang, Z., Bogdal, C., Scheringer, M., Hungerbühler, K., 2016. Global production, use, and emission volumes of short-chain chlorinated paraffins – a minimum scenario. Sci. Total Environ. 573, 1132–1146.

Gong, P., Xu, H., Wang, C., Chen, Y., Guo, L., Wang, X., 2021. Persistent organic pollutant cycling in forests. Nat. Rev. Earth Environ. 2 (3), 182–197.

Huang, H., Gao, L., Xia, D., Qiao, L., 2017. Bioaccumulation and biomagnification of short and medium chain polychlorinated paraffins in different species of fish from Liaodong Bay. North China. Sci Rep 7, 10749.

Iozza, S., Schmid, P., Oehme, M., Bassan, R., Belis, C., Jakobi, G., Kirchner, M., Schramm, K.-W., Kräuchi, N., Moche, W., Offenthaler, I., Weiss, P., Simončič, P., Knoth, W., 2009. Altitude profiles of total chlorinated paraffins in humus and spruce needles from the Alps (MONARPOP). Environ. Pollut. 157 (12), 3225–3231.

Jury, W.A., Spencer, W.F., Farmer, W.J., 1983. Behavior assessment model for trace organics in soil: I. J. Environ. Qual. 12 (4) https://doi.org/10.2134/jeq1983.00472425001200040026x.

Li, Q., Li, J., Wang, Y., Xu, Y., Pan, X., Zhang, G., Luo, C., Kobara, Y., Nam, J.-J., Jones, K. C., 2012. Atmospheric short-chain chlorinated paraffins in China, Japan, and South Korea. Environ. Sci. Technol. 46 (21), 11948–11954.

Li, Q., Wang, Y., Luo, C., Li, J., Zhang, G., 2015. Characterization and risk assessment of polychlorinated biphenyls in soils and rice tissues in a suburban paddy field of the Pearl River Delta, South China. Environ. Sci. Pollut. Res. Int. 22 (15), 11626–11633.

Li, Y., Chen, W., Kong, W., Liu, J., Schnoor, J.L., Jiang, G., 2020. Transformation of 1,1,1,3,8,10,10,10-octachlorodecane in air phase increased by phytogenic volatile organic compounds of pumpkin seedlings. Sci. Total Environ. 704, 135455. https://doi.org/10.1016/j.scitotenv.2019.135455.

Li, Y., Hou, X., Chen, W., Liu, J., Zhou, Q., Schnoor, J.L., Jiang, G., 2019. Carbon chain decomposition of short chain chlorinated paraffins mediated by pumpkin and soybean seedlings. Environ. Sci. Technol. 53 (12), 6765–6772.

Li, Y., Hou, X., Yu, M., Zhou, Q., Liu, J., Schnoor, J.L., Jiang, G., 2017. Dechlorination and chlorine rearrangement of 1,2,5,5,6,9,10-heptachlorodecane mediated by the whole pumpkin seedlings. Environ. Pollut. 224, 524–531.

Liu, D.i., Li, Q., Cheng, Z., Li, K., Li, J., Zhang, G., 2020. Spatiotemporal variations of chlorinated paraffins in PM2.5 from Chinese cities: implication of the shifting and upgrading of its industries. Environ. Pollut. 259, 113853. https://doi.org/10.1016/j.envpol.2019.113853.

Meng, B.o., Feng, X., Qiu, G., Liang, P., Li, P., Chen, C., Shang, L., 2011. The process of methylmercury accumulation in rice (Oryza sativa L.). Environ. Sci. Technol. 45 (7), 2711–2717.

Peng, S., Tang, Q., Zou, Y., 2008. Current status and challenges of rice production in China. Plant Prod. Sci. 12 (1), 3–8.

Qiao, L., Gao, L., Xia, D., Huang, H., Zheng, M., 2017. Short- and medium-chain chlorinated paraffins in sediments from the middle reaches of the Yangtze River: spatial distributions, source apportionment and risk assessment. Sci. Total Environ. 575, 1177–1182.

Qiao, L., Gao, L., Zheng, M., Xia, D., Li, J., Zhang, L., Wu, Y., Wang, R., Cui, L., Xu, C., 2018. Mass fractions, congener group patterns, and placental transfer of short- and medium-chain chlorinated paraffins in paired maternal and cord serum. Environ. Sci. Technol. 52 (17), 10097–10103.

Takaki, K., Wade, A.J., Collins, C.D., 2014. Assessment of plant uptake models used in exposure assessment tools for soils contaminated with organic pollutants. Environ. Sci. Technol. 48 (20), 12073–12082.

Tomy, G.T., Fisk, A.T., Westmore, J.B., Muir, D.C., 1998. Environmental chemistry and toxicology of polychlorinated n-alkanes. Rev. Environ. Contam. Toxicol. 158, 53–128.

Trapp, S., Matthies, M., 1995. Generic one-compartment model for uptake of organic chemicals by foliar vegetation. Environ. Sci. Technol. 29 (9), 2333–2338.

UNEP. POPS/COP.8/CRP.13, 2017. Draft decision SC-8/[ ]: Short-chain chlorinated paraffins.

USEPA, 2000. Risk characterization handbook.

van Mourik, L.M., Gaus, C., Leonards, P.E.G., de Boer, J., 2016. Chlorinated paraffins in the environment: a review on their production, fate, levels and trends between 2010 and 2015. Chemosphere 155, 415–428.

Wang, H., Chang, H., Zhang, C., Feng, C., Wu, F., 2021. Occurrence of chlorinated Paraffins in a wetland ecosystem: removal and distribution in plants and sediments. Environ. Sci. Technol. 55 (2), 994–1003.

Wang, T., Yu, J., Han, S., Wang, Y., Jiang, G., 2015a. Levels of short chain chlorinated Paraffins in pine needles and bark and their vegetation-air partitioning in urban areas. Environ. Pollut. 196, 309–312.

Wang, X.-T., Zhou, J., Lei, B.-L., Zhou, J.-M., Xu, S.-Y., Hu, B.-P., Wang, D.-Q., Zhang, D.-P., Wu, M.-H., 2016. Atmospheric occurrence, homologue patterns and source apportionment of short- and medium-chain chlorinated paraffins in Shanghai, China: Biomonitoring with Masson pine (Pinus massoniana L.) needles. Sci. Total Environ. 560-561, 92–100.

Wang, Y., Luo, C., Wang, S., Liu, J., Pan, S., Li, J., Ming, L., Zhang, G., Li, X., 2015b. Assessment of the air-soil partitioning of polycyclic aromatic hydrocarbons in a paddy field using a modified fugacity sampler. Environ. Sci. Technol. 49 (1), 284–291.

Xia, D., Vaye, O., Lu, R., Sun, Y., 2021. Resolving mass fractions and congener group patterns of C8–C17 chlorinated paraffins in commercial products: associations with source characterization. Sci. Total Environ. 769, 144701. https://doi.org/10.1016/j.scitotenv.2020.144701.

Xin, S., Gao, W., Wang, Y., Jiang, G., 2017. Thermochemical emission and transformation of chlorinated paraffins in inert and oxidizing atmospheres. Chemosphere 185, 899–906.

Xu, S.B., Li, T., Deng, Z.Y., Chong, K., Xue, Y., Wang, T., 2008. Dynamic proteomic analysis reveals a switch between central carbon metabolism and alcoholic fermentation in rice filling grains. Plant Physiol. 148, 908–925.

Yuan, B.o., Alsberg, T., Bogdal, C., MacLeod, M., Berger, U., Gao, W., Wang, Y., de Wit, C. A., 2016. Deconvolution of soft ionization mass spectra of chlorinated paraffins to resolve congener groups. Anal. Chem. 88 (18), 8980–8988.

Yuan, B.o., Fu, J., Wang, Y., Jiang, G., 2017a. Short-chain chlorinated paraffins in soil, paddy seeds (*Oryza sativa*) and snails (*Ampullariidae*) in an e-waste dismantling area in China: Homologue group pattern, spatial distribution and risk assessment. Environ. Pollut. 220, 608–615.

Yuan, B.o., McLachlan, M.S., Roos, A.M., Simon, M., Strid, A., de Wit, C.A., 2021a. Long-chain chlorinated Paraffins have reached the arctic. Environ. Sci. Technol. Lett. 8 (9), 753–759.

Yuan, B.o., Muir, D., MacLeod, M., 2019a. Methods for trace analysis of short-, medium-, and long-chain chlorinated Paraffins: critical review and recommendations. Anal. Chim. Acta 1074, 16–32.

Yuan, B.o., Strid, A., Darnerud, P.O., de Wit, C.A., Nyström, J., Bergman, Å., 2017b. Chlorinated paraffins leaking from hand blenders can lead to significant human exposures. Environ. Int. 109, 73–80.

Yuan, B.o., Tay, J.H., Padilla-Sánchez, J.A., Papadopoulou, E., Haug, L.S., de Wit, C.A., 2021b. Human exposure to chlorinated Paraffins via inhalation and dust ingestion in a norwegian cohort. Environ. Sci. Technol. 55 (2), 1145–1154.

Yuan, B.o., Vorkamp, K., Roos, A.M., Faxneld, S., Sonne, C., Garbus, S.E., Lind, Y., Eulaers, I., Hellström, P., Dietz, R., Persson, S., Bossi, R., de Wit, C.A., 2019b. Accumulation of short-, medium-, and long-chain chlorinated paraffins in marine and terrestrial animals from scandinavia. Environ. Sci. Technol. 53 (7), 3526–3537.

Zhang, Y., Luo, X.-J., Mo, L., Wu, J.-P., Mai, B.-X., Peng, Y.-H., 2015. Bioaccumulation and translocation of polyhalogenated compounds in rice (Oryza sativa L.) planted in paddy soil collected from an electronic waste recycling site, South China. Chemosphere 137, 25–32.

Zhao, L.P., Tao, Y.S., Tang, Y.P., Tang, Q.Y., 2013. The evolution history and development trend of Rice's cultivation methods. Crop Res.

Zhao-Wei, L.I., Xiong, J., Xiao-Hui, Q.I., Wang, J.Y., Lin, W.X., 2009. Differential expression and function analysis of proteins in flag leaves of rice during grain filling. Acta Agron. Sinica 35, 132–139.

Zhou, Y., de Wit, C.A., Yin, G.e., Du, X., Yuan, B.o., 2019. Shorter than short-chain: Very short-chain chlorinated paraffins (vSCCPs) found in wildlife from the Yangtze River Delta. Environ. Int. 130, 104955. https://doi.org/10.1016/j.envint.2019.104955.

Zhou, Y., Yuan, B.o., Nyberg, E., Yin, G.e., Bignert, A., Glynn, A., Odland, J.Ø., Qiu, Y., Sun, Y., Wu, Y., Xiao, Q., Yin, D., Zhu, Z., Zhao, J., Bergman, Å., 2020. Chlorinated Paraffins in human milk from urban sites in China, Sweden, and Norway. Environ. Sci. Technol. 54 (7), 4356–4366.

Zou, Y., Niu, S., Dong, L., Hamada, N., Hashi, Y., Yang, W., Xu, P., Arakawa, K., Nagata, J., 2018. Determination of short-chain chlorinated paraffins using comprehensive two-dimensional gas chromatography coupled with low resolution mass spectrometry. J. Chromatogr. A 1581, 135–143.